ChemComm

COMMUNICATION

View Article Online
View Journal | View Issue

Cite this: *Chem. Commun.*, 2019, **55**, 3359

Received 28th December 2018,
Accepted 15th February 2019

DOI: 10.1039/c8cc10260k

rsc.li/chemcomm

Room temperature hysteretic spin crossover in a new cyanoheterometallic framework†

Volodymyr M. Hiiuk,[abc] Sergiu Shova,[d] Aurelian Rotaru,[e] Vadim Ksenofontov,[f] Igor O. Fritsky[ab] and Il'ya A. Gural'skiy[*ab]

A new iron(II)-based spin-crossover compound with thermal hysteresis operating under ambient conditions is reported. This complex exhibits a high reproducibility of the spin transition in many successive thermal cycles, stability of both spin states at room temperature and an attractive operational temperature range.

The spin crossover (SCO) is an intrinsically interesting electronic phenomenon,[1] which is a characteristic of some 3d metal complexes. In such materials, the electronic state can be tuned from low spin (LS) configuration to a metastable high spin (HS) configuration through external stimuli: thermally, by the influence of a magnetic field, light irradiation, pressure or through absorption of guest molecules.[2] Among the possible types of spin transitions (gradual, multistep, abrupt, hysteretic, incomplete), most attention is focused on the bistability in highly cooperative systems with thermal hysteresis.[3] Such compounds can exist in two different electronic states at the same external conditions, having different magnetic, electrical[4] and mechanical properties.[5] The presence of bistability makes them ideal components for making a new generation of devices in molecular memories and switches. In order to reach this goal, this transition needs to occur at room temperature (RT), be reversible and stable through cycling. Most examples of spin-crossover systems that meet these requirements are based on iron(II) complexes.[6] A nice example is the spin-crossover complex that has a 70 K hysteresis centred at 279 K.[7] Another remarkable example includes a compound that has a spin-crossover behaviour with a narrow hysteresis in the temperature range of 285–287 K (ΔT_c = 2 K).[8] It is worth noting coordination polymers of composition $[Fe(pz)Ni(CN)_4]\cdot 2H_2O$ (280–305 K) and $[Fe(pz)Pd(CN)_4]\cdot 1.5H_2O\cdot 0.5(CS(NH_2)_2)$ (273–304 K).[9] However, spin-crossover characteristics of these complexes depend on the presence of the solvate molecules. Most of the SCO materials with a hysteresis loop known to date display a spin transition at low temperatures or at high temperatures.[10] In recent years, synthetic strategies for obtaining spin-crossover materials offered the creation of complicated chemical systems, which require the use of hard-to-synthesize ligands.[11] At the same time, Hofmann-like polymeric SCO complexes, that are much easier to synthesize, can be used to obtain spin-transition materials with thermal hysteresis. Variety of such complexes originates from a set of available azine ligands and cyanometalates.[12]

Here we report on the successful synthesis of a cyanoheterometallic coordination polymer with a bicyclic ligand 1,6-naphthyridine (1,6-naphthy) of composition $[Fe(1,6\text{-naphthy})_2(Ag(CN)_2)_2]$ (**1**) with a 19 K wide thermal hysteresis centred near RT (297 K).

We found that all crystals of **1** crystallize at RT in the LS form. Further heating to 310 K causes the change of the crystal colour from red to orange that is related to the LS → HS transition. Upon cooling to RT the spin state of the complex remains HS.

Single crystals of **1** used for X-ray diffraction were obtained by a slow diffusion method between an aqueous solution of cyanometallate and 1,6-naphthy, from one side, and ethanolic solution of $Fe(OTs)_2\cdot 6H_2O$ (OTs = *p*-toluenesulphonate), from another side. XRD experiments were carried out for **1** at 293 K in the hysteresis loop that allowed to obtain two structures of the same crystal – in LS and HS states at RT. A selection of bond lengths [Å], angles [°] and relevant crystallographic data is given in Table 1. The structural analysis of **1** showed that it crystallizes in the orthorhombic *Pbca* space group for both states

[a] *Department of Chemistry, Taras Shevchenko National University of Kyiv, 64 Volodymyrska St., 01601 Kyiv, Ukraine. E-mail: illia.guralskyi@univ.kiev.ua*
[b] *UkrOrgSyntez Ltd., 67 Chervonotkatska St., 02094 Kyiv, Ukraine*
[c] *Faculty of Natural Sciences, National University of Kyiv-Mohyla Academy, 2 Skovorody St., 04070 Kyiv, Ukraine*
[d] *"Petru Poni" Institute of Macromolecular Chemistry, 41A Aleea Gr. Ghica Voda, 700487 Iasi, Romania*
[e] *Faculty of Electrical Engineering and Computer Science & Research Center MANSiD, Stefan cel Mare University, 13 Universitatii St., 720229 Suceava, Romania*
[f] *Institute of Inorganic and Analytical Chemistry, Johannes Gutenberg University of Mainz, Duesbergweg 10–14, Mainz 55099, Germany*

† Electronic supplementary information (ESI) available: Synthesis, crystallization, PXRD, IR, magnetic, Mössbauer, optical, calorimetric measurements, simulations, crystal data and refinement details. CCDC 1878181 (1^{LS}) and 1878182 (1^{HS}). For ESI and crystallographic data in CIF or other electronic format see DOI: 10.1039/c8cc10260k

Table 1 Selected crystallographic data for $\mathbf{1}^{LS}$ and $\mathbf{1}^{HS}$ at 293 K

	$\mathbf{1}^{LS}$ (293 K)	$\mathbf{1}^{HS}$ (293 K)
a (Å)	14.4739(8)	15.1721(15)
b (Å)	13.8064(7)	14.0669(12)
c (Å)	20.7510(11)	21.0860(2)
V (Å^3)	4146.7(4)	4500.2(7)
Fe1–N1 (Å)	1.926(8)	2.096(10)
Fe1–N2 (Å)	1.944(7)	2.135(10)
Fe1–N3 (Å)	1.973(8)	2.112(10)
Fe1–N4 (Å)	1.959(7)	2.123(10)
Fe1–N5 (Å)	2.008(7)	2.197(10)
Fe1–N6 (Å)	2.008(7)	2.196(10)
Ag2–N7^{iii} (Å)	2.396(7)	2.514(7)
Ag2–Ag1^{iv} (Å)	3.077(10)	3.089(15)
C1^{v}–Ag2–N7^{iii} (°)	92.4(3)	93.5(4)
C4–Ag2–N7^{iii} (°)	124.8(3)	113.2(4)
Σ (°)	10.3	10.9
V_{octa}	10.18	13.11

Symmetry codes for $\mathbf{1}^{LS}$: (iii) $1-x, -0.5+y, 0.5-z$; (iv) $-0.5+x, 1.5-y, 1-z$; (v) $1.5-x, -1.5+y, z$.

($\mathbf{1}^{LS}$ and $\mathbf{1}^{HS}$). Iron has a coordination environment of an elongated [FeN$_6$] pseudo-octahedron (Fig. 1a).

The thermally induced spin transition is always accompanied by significant structural changes in the metal coordination environment. The occupancies of the antibonding e_g* orbitals in the HS state reduce the multiplicity of the metal–ligand bond, while reduction of the occupancies of the nonbonding t_{2g} sublevel reduces the π-dative interaction between the metal ion and the vacant π*-orbitals of ligand. Both factors contribute to an increase in the metal–ligand bond length for Fe by ∼10% (∼0.2 Å). The average bond length ⟨Fe–N⟩ is 1.970(7) Å and 2.143(10) Å for $\mathbf{1}^{LS}$ and $\mathbf{1}^{HS}$, while the volume of FeN$_6$ octahedron changes from 10.18 to 13.11 Å^3 upon SCO. The Fe–N lengths distinction of *ca.* 0.173 Å between the LS and HS states is consistent with a complete spin transition.

As expected, the cell parameters increase upon LS to HS transition (Δa = +4.82%, Δb = +1.89% and Δc = +1.61%) and the volume of the unit cell grows by 8.5%. Significant volume changes associated with the SCO phenomenon are of particular interest. For example, molecular switches are perspective to produce artificial muscles and alternative transductors for MEMS and NEMS devices.[13]

The sum of deviations from the ideal octahedron of the 12 "*cis*" N–Fe–N angles ($\Sigma = |90^\circ - \theta_{N-Fe-N}|$) shows that the coordination geometry around the Fe centre is some distorted in the HS state with $\Sigma = 10.9^\circ$ and this value decreases slightly in the LS state down to 10.3°. This insignificant difference signalize that the octahedral distortion parameter is not always characteristic for monitoring the spin state change.

Complex **1** contains one Fe^{II} centre, whereas two independent Ag atoms belong to the asymmetric unit. Each iron atom is equatorially coordinated by two equivalent pairs of crystallographically independent [Ag(CN)$_2$]$^-$ groups. Dicyanoargentate is more bent for Ag2 (in LS C–Ag1–C is 169.2(3)°, C–Ag2–C is 142.7(3)°), but this difference decreases upon SCO (in HS C–Ag1–C is 170.6(5)°, C–Ag2–C is 153.3(5)°). Two crystallographically non-equivalent 1,6-naphthy ligands bind axially to each Fe^{II} site, completing its octahedral coordination environment (Fig. 1a). The 2D network of the complex consists of two (4,4)-nets of {Fe(Ag(CN)$_2$)$_2$} which lie parallel to the *ab*-plane and are connected by *N*,*N*′-bridging 1,6-naphthy ligands that link Fe1 of one layer to Ag2 of another layer (Fig. 1b and Fig. S1, S2, ESI†). This Ag2–N7^{ii} distance varies substantially with SCO (2.396(7) in LS *vs.* 2.514(7) in HS). The 2D layers of the structure are connected by strong argentophilic interactions and π–π stacking (Fig. 1c and Fig. S2, ESI†). The Ag···Ag distance (3.077(10) Å for $\mathbf{1}^{LS}$ *vs.* 3.089(15) Å for $\mathbf{1}^{HS}$) is insensitive to the SCO, while in analogues cyanometallic structures considerable changes are known. The presence of strong homoatomic metal–metal interactions may play an important role in increasing the dimensionality and rigidity of a structure. These supramolecular features are found responsible for the cooperativity of SCO in some compounds.[14] Dense packing ensured by bridging ligand molecules and π–π stacking is responsible for no voids available in the structure **1**.

Real *et al.* have obtained a compound of similar composition [Fe(2,6-naphthy)[Ag(CN)$_2$]Ag$_2$(CN)$_3$] using the structural isomer of 1,6-naphthy – 2,6-naphthyridine (2,6-naphthy).[15] Such isomerization of the ligand leads to a completely different topology of

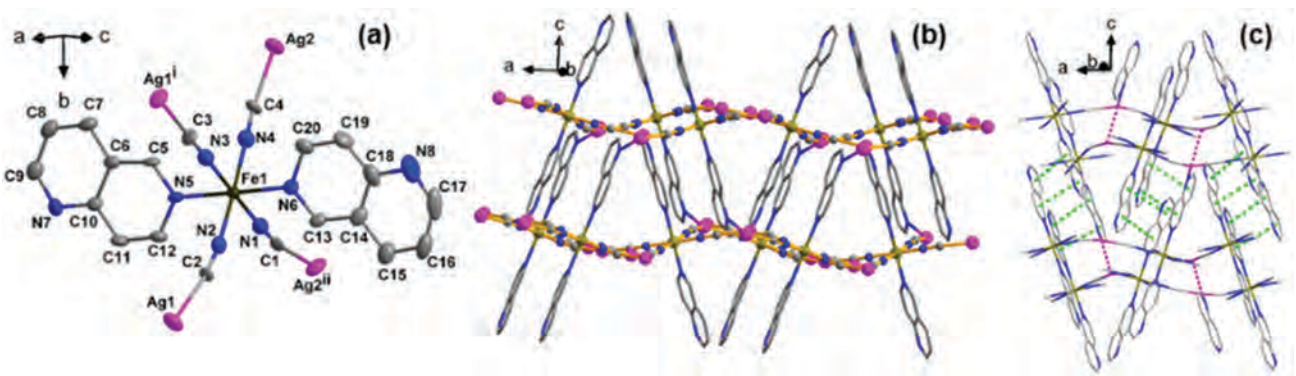

Fig. 1 Crystal structure of **1**: (a) representation of fragment of complex **1** (thermal ellipsoids are given at 50% probability). Symmetry codes: (i) $1.5-x, -0.5+y, z$; (ii) $0.5-x, 0.5+y, z$; (b) 2D crystal framework view along the [010] direction; (c) supramolecular packing *via* Ag–Ag (pink) and π–π (green) interactions.

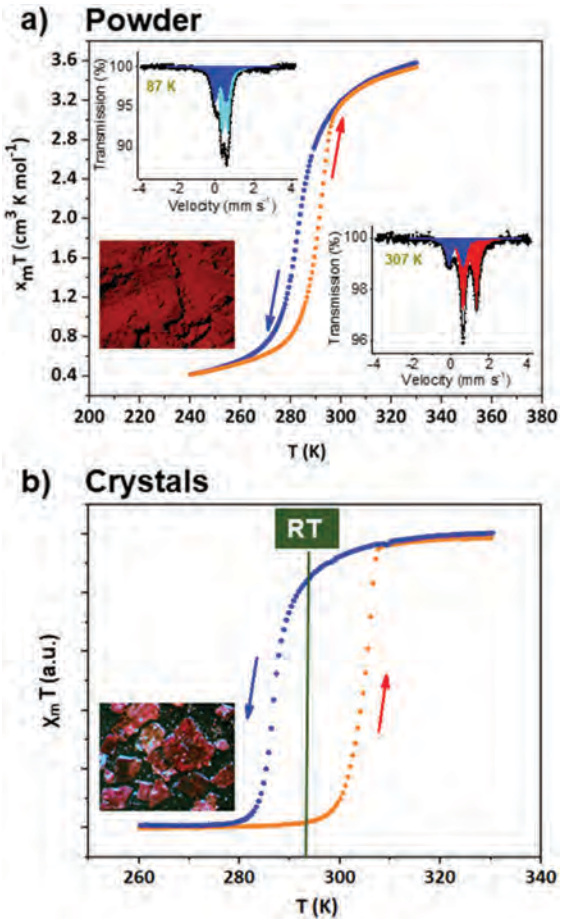

Fig. 2 (a) Thermal variation of the $\chi_M T$ product for $\mathbf{1}_{powd}$: the LS to HS transition occurs at 293 K, the HS to LS transition takes place at 283 K. The measurements were carried out at a 3 K min^{-1} under the field of 0.5 T. Mössbauer spectra at 87 and 307 K are inserted. (b) Temperature dependence of $\chi_M T$ for $\mathbf{1}_{cryst}$, scaled to γ_{HS}, measured at a 3 K min^{-1} under the field of 0.1 T. The LS to HS transition occurs at 306 K, the HS to LS transition takes place at 287 K.

framework, which, in its turn, leads to a sharp difference in the spin-crossover properties.

The spin transition in Fe^{II} causes the change of the total spin between S = 0 for the LS state and S = 2 for the HS state. Such a transition is accompanied by a significant increase of magnetic susceptibility of the system; therefore, the measurement of this change was and remains an important method of observing the spin transition. The magnetic properties of **1** were determined by temperature-dependent magnetic susceptibility measurements using a SQUID magnetometer. The thermal dependence of $\chi_M T$ for **1** is shown in Fig. 2. Magnetic measurements were performed for the bulk powder ($\mathbf{1}_{powd}$) and for the single crystals ($\mathbf{1}_{cryst}$).

Dependence of magnetic susceptibility on temperature for powder at 240–330 K is given in Fig. 2a. At 330 K, the $\chi_M T$ of $\mathbf{1}_{powd}$ is 3.53 cm^3 mol^{-1} K, indicating the sample is in the HS state.[9a] Upon cooling, a spin transition to the low-spin state is observed and $\chi_M T$ is 0.41 cm^3 mol^{-1} K at 240 K. Notably, the spin change occurs near RT with $T_c\downarrow$ = 283 K and $T_c\uparrow$ = 293 K in the cooling and heating cycles, respectively (hysteresis loop of *ca.* 10 K wide). Mössbauer spectra of $\mathbf{1}_{powd}$ at 87 and 307 K are shown in Fig. 2a. Two slightly resolved LS centres are detected at low temperature (LS1: δ = 0.245(7) mm s^{-1} and ΔE_Q = 0.591(11) mm s^{-1}; LS2: δ = 0.472(3) mm s^{-1} and ΔE_Q = 0.320(8) mm s^{-1}) with LS1 : LS2 ratio of 41(3) : 59(2). These centres are not structurally resolved, but have different Mössbauer parameters. At 307 K the SCO is not yet accomplished, since only 70(2)% of Fe(II) is converted into HS form (HS: δ = 0.99(3) mm s^{-1} and ΔE_Q = 0.71(6) mm s^{-1}) (Table S1, ESI†).

Magnetic properties of $\mathbf{1}_{cryst}$ in the temperature range of 260–330 K are shown in Fig. 2b. The $\chi_M T$ values are given in arbitrary units, since they cannot be correctly measured due to a small quantity of crystals (Fig. S3, ESI†). The spin change occurs exactly around RT with $T_c\downarrow$ = 287 K and $T_c\uparrow$ = 306 K in the cooling and heating cycles, respectively. 19 K wide thermal hysteresis centred precisely at 297 K is observed.

The presence of a thermal hysteresis loop clearly demonstrates the existence of a significant level of cooperativity for the bulk powder and for the single crystals. Considering PXRD (Fig. S4, ESI†) and IR (Fig. S5, ESI†) reveal the crystals and powder are of the same compound, minor difference in transition temperatures, width and sharpness of hysteresis for $\mathbf{1}_{cryst}$ and $\mathbf{1}_{powd}$ should be attributed to a different degree of cooperativity in the systems. Thus, Slichter–Drickamer simulations of the spin transitions curves (Fig. S6, ESI†) reveal the interaction terms Γ of 6200 J mol^{-1} ($\mathbf{1}_{cryst}$) and 4900 J mol^{-1} ($\mathbf{1}_{powd}$), that quantify this decrease of cooperativity.

Thermally induced SCO is always accompanied by a change in the colour. The change of colour of substances upon temperature is referred as thermochromism. The colours of HS and LS complexes can be attributed to d–d and MLCT electronic transitions that change upon SCO. This allows us to observe the spin transition by the change of intensity of the reflected light. The characteristic curve (Fig. 3a) confirms the presence of a spin transition at RT, the values of transition temperatures ($T_c\downarrow$ = 292 K and $T_c\uparrow$ = 311 K) are consistent with the values obtained by magnetic measurements. A shift in temperature comparing to magnetic measurements is related to a different thermalisation coming from different heating/cooling rates (10 K min^{-1} in optical *vs.* 3 K min^{-1} in magnetic). Optical and magnetic data are also supported by DSC-revealed thermal effects of transition (Fig. S7, ESI†).

Conventional reversible thermochromic materials change their colour at a certain temperature. At one temperature, materials assume only one of two colours. Due to the hysteresis, SCO complexes usually can retain the colour of the HS or LS state at the same temperature. In our case, this allows the production of materials with "thermochromic memory" at RT. Moreover, this colour change is highly reversible by slight heating or cooling. Therefore, this type of materials is powerful for practical applications, such as temperature-sensitive recording materials, thermochromic indicators, as labels in engineering processes, in protective elements and printing materials. The stability of both spin states of **1** at RT and reproducibility of state change are essential characteristics for application of SCO materials.

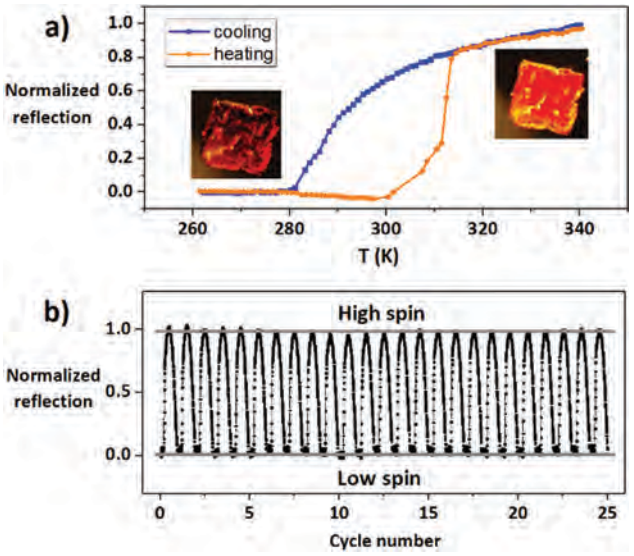

Fig. 3 (a) Change in the intensity of reflected light for complex **1** related to the cooperative spin transition. Heating/cooling rate is 10 K min^{-1}; (b) reproducibility of state change between the LS and HS upon successive thermal cycles. Every thermal cycle corresponds to 343 K → 258 K → 343 K sequence (heating/cooling rate is 20 K min^{-1}).

Therefore, to confirm the effectiveness of our spin-crossover material over time we carried out optical measurements in 25 consecutive cycles with a rate of temperature change of 20 K min^{-1} (Fig. 3b) (even though it can operate in many more cycles, the experiment was limited in time). The last thermal profiles are perfectly consistent with the initial cycles. High reproducibility of successive thermal cycles can eventually allow the development of highly efficient devices due to stability of the SCO behaviour.

In summary, we obtained a new cyanoheterometallic coordination polymer of the composition $[Fe(1,6\text{-naphthy})_2(Ag(CN)_2)_2]$ with a thermal hysteresis of 19 K width centred at room temperature (297 K). It is noteworthy that the LS and HS structures of **1** were determined at 293 K in the hysteresis loop for the same crystal. Remarkably, the complex **1** exhibits a high reproducibility of the spin transition in many successive thermal cycles, stability of both spin states at the same temperature and an attractive operational temperature range. The presence of a thermal hysteresis at RT provides bistability of numerous characteristics, including magnetic, optical, structural and some other (that will become a topic of further investigations of this compound).

This work was supported by H2020-MSCA-RISE-2016 Project 734322 and Projects DZ/55-2018 and 19BF037-01M of the Ministry of Education and Science of Ukraine. V. Hiiuk thanks Yuchymenko Family Endowement for the financial support. A. Rotaru acknowledges the CNFIS for CNFIS-FDI-2018-058 project.

Conflicts of interest

There are no conflicts to declare.

Notes and references

1 (*a*) P. Gütlich, Y. Garcia and H. A. Goodwin, *Chem. Soc. Rev.*, 2000, **29**, 419–427; (*b*) K. Senthil Kumar and M. Ruben, *Coord. Chem. Rev.*, 2017, **346**, 176–205.
2 (*a*) L. Cambi and L. Szegö, *Ber. Dtsch. Chem. Ges.*, 1931, **64**, 2591–2598; (*b*) V. Niel, M. C. Muñoz, A. B. Gaspar, A. Galet, G. Levchenko and J. A. Real, *Chem. – Eur. J.*, 2002, **8**, 2446; (*c*) Y. Qi, E. W. Müller, H. Spiering and P. Gütlich, *Chem. Phys. Lett.*, 1983, **101**, 503–505; (*d*) P. Gütlich, A. Hauser and H. Spiering, *Angew. Chem., Int. Ed. Engl.*, 1994, **33**, 2024–2054; (*e*) P. Gütlich, V. Ksenofontov and A. B. Gaspar, *Coord. Chem. Rev.*, 2005, **249**, 1811–1829; (*f*) M. Ohba, K. Yoneda, G. Agustí, M. C. Muñoz, A. B. Gaspar, J. A. Real, M. Yamasaki, H. Ando, Y. Nakao, S. Sakaki and S. Kitagawa, *Angew. Chem., Int. Ed.*, 2009, **48**, 4767–4771.
3 (*a*) X. Bao, H. J. Shepherd, L. Salmon, G. Molnár, M.-L. Tong and A. Bousseksou, *Angew. Chem., Int. Ed.*, 2013, **52**, 1198–1202; (*b*) S. Brooker, *Chem. Soc. Rev.*, 2015, **44**, 2880–2892; (*c*) A. Bousseksou, G. Molnár, L. Salmon and W. Nicolazzi, *Chem. Soc. Rev.*, 2011, **40**, 3313.
4 (*a*) F. Prins, M. Monrabal-Capilla, E. A. Osorio, E. Coronado and H. S. J. van der Zant, *Adv. Mater.*, 2011, **23**, 1545–1549; (*b*) C. Etrillard, V. Faramarzi, J.-F. Dayen, J.-F. Letard and B. Doudin, *Chem. Commun.*, 2011, **47**, 9663; (*c*) A. Rotaru, I. A. Gural'skiy, G. Molnár, L. Salmon, P. Demont and A. Bousseksou, *Chem. Commun.*, 2012, **48**, 4163–4165; (*d*) A. Rotaru, J. Dugay, R. P. Tan, I. A. Guralskiy, L. Salmon, P. Demont, J. Carrey, G. Molnár, M. Respaud and A. Bousseksou, *Adv. Mater.*, 2013, **25**, 1745–1749.
5 (*a*) H. J. Shepherd, I. A. Gural'skiy, C. M. Quintero, S. Tricard, L. Salmon, G. Molnár and A. Bousseksou, *Nat. Commun.*, 2013, **4**, 2607; (*b*) I. A. Gural'skiy, C. M. Quintero, J. S. Costa, P. Demont, G. Molnár, L. Salmon, H. J. Shepherd and A. Bousseksou, *J. Mater. Chem. C*, 2014, **2**, 2949–2955; (*c*) M. Mikolasek, M. D. Manrique-Juarez, H. J. Shepherd, K. Ridier, S. Rat, V. Shalabaeva, A.-C. Bas, I. E. Collings, F. Mathieu, J. Cacheux, T. Leichle, L. Nicu, W. Nicolazzi, L. Salmon, G. Molnár and A. Bousseksou, *J. Am. Chem. Soc.*, 2018, **140**, 8970–8979.
6 I. Šalitroš, N. T. Madhu, R. Boča, J. Pavlik and M. Ruben, *Monatsh. Chem.*, 2009, **140**, 695–733.
7 B. Weber, W. Bauer and J. Obel, *Angew. Chem., Int. Ed.*, 2008, **47**, 10098–10101.
8 C. Rajadurai, F. Schramm, S. Brink, O. Fuhr, M. Ghafari, R. Kruk and M. Ruben, *Inorg. Chem.*, 2006, **45**, 10019–10021.
9 (*a*) V. Niel, J. M. Martinez-Agudo, M. C. Muñoz, A. B. Gaspar and J. A. Real, *Inorg. Chem.*, 2001, **40**, 3838–3839; (*b*) F. J. Muñoz Lara, A. B. Gaspar, D. Aravena, E. Ruiz, M. C. Muñoz, M. Ohba, R. Ohtani, S. Kitagawa and J. A. Real, *Chem. Commun.*, 2012, **48**, 4686.
10 (*a*) I. A. Gural'skiy, B. O. Golub, S. I. Shylin, V. Ksenofontov, H. J. Shepherd, P. R. Raithby, W. Tremel and I. O. Fritsky, *Eur. J. Inorg. Chem.*, 2016, 3191–3195; (*b*) I. A. Gural'skiy, S. I. Shylin, B. O. Golub, V. Ksenofontov, I. O. Fritsky and W. Tremel, *New J. Chem.*, 2016, **40**, 9012–9016.
11 (*a*) C. Rajadurai, O. Fuhr, R. Kruk, M. Ghafari, H. Hahn and M. Ruben, *Chem. Commun.*, 2007, 2636; (*b*) L.-F. Qin, C.-Y. Pang, W.-K. Han, F.-L. Zhang, L. Tian, Z.-G. Gu, X. Ren and Z. Li, *Dalton Trans.*, 2016, **45**, 7340–7348; (*c*) M. A. Halcrow, *Crystals*, 2016, **6**, 58.
12 (*a*) M. C. Muñoz and J. A. Real, *Coord. Chem. Rev.*, 2011, **255**, 2068–2093; (*b*) Z.-P. Ni, J.-L. Liu, M. N. Hoque, W. Liu, J.-Y. Li, Y.-C. Chen and M.-L. Tong, *Coord. Chem. Rev.*, 2017, **335**, 28–43.
13 (*a*) M. D. Manrique-Juárez, S. Rat, L. Salmon, G. Molnár, C. M. Quintero, L. Nicu, H. J. Shepherd and A. Bousseksou, *Coord. Chem. Rev.*, 2016, **308**, 395–408; (*b*) K. Eom, H. Jung, G. Lee, J. Park, K. Nam, S. W. Lee, D. S. Yoon, J. Yang and T. Kwon, *Chem. Commun.*, 2012, **48**, 955–957.
14 T. Kosone, Y. Suzuki, S. Ono, C. Kanadani, T. Saito and T. Kitazawa, *Dalton Trans.*, 2010, **39**, 1786.
15 L. Piñeiro-López, F. J. Valverde-Muñoz, M. Seredyuk, C. Bartual-Murgui, M. C. Muñoz and J. A. Real, *Eur. J. Inorg. Chem.*, 2018, 289–296.

